2015

Effects of Non-Uniform Heating on the Location and Magnitude of Critical Heat Flux in a Microchannel Heat Sink

S. N. Ritchey
Purdue University

J. A. Weibel
Purdue University, jaweibel@purdue.edu

S V. Garimella
Purdue University, sureshg@purdue.edu

Effects of Non-Uniform Heating on the Location and Magnitude of Critical Heat Flux in a Microchannel Heat Sink

by

Susan N. Ritchey, Justin A. Weibel
and Suresh V. Garimella

reprinted from

International Journal of
Micro-Nano
Scale Transport

Volume 5 · Number 3 · September 2014

Multi-Science Publishing
ISSN 1759-3093

Effects of Non-Uniform Heating on the Location and Magnitude of Critical Heat Flux in a Microchannel Heat Sink

Susan N. Ritchey, Justin A. Weibel and Suresh V. Garimella
Cooling Technologies Research Center, an NSF I/UCRC, School of Mechanical Engineering
Purdue University, 585 Purdue Mall, West Lafayette, IN 47907 USA
sureshg@purdue.edu

Abstract

Decreasing form factors and diminishing numbers of thermal interfaces and spreading layers in modern, compact electronic packages result in non-uniform heat generation profiles at the chip level being transmitted directly to the heat sinks. An improved understanding of the effects of non-uniform heating on the heat dissipation limits in microchannel heat sinks has become essential. An experimental investigation is conducted to measure the location and magnitude of critical heat flux (CHF) in a microchannel heat sink exposed to a range of non-uniform heating profiles. A 12.7 mm $\times$ 12.7 mm silicon microchannel heat sink with an embedded 5×5 array of individually controllable heaters is used in the experiments. The microchannels in the heat sink are 240 mm wide and 370 μm deep, and are separated by 110 mm wide fins. The dielectric fluid HFE-7100 is used as the coolant, with an average mass flux in the heat sink of approximately 800 kg/m^{2}s. High-speed visualizations of the flow are recorded to capture the CHF phenomena observed. A central 'hotspot' spanning the entire length of the heat sink in the flow direction (formed by heating only the central 20 percent of the base area) produced both the largest wall excess temperature and the lowest CHF of all the heat flux distributions investigated, due to the flow maldistribution induced. A single transverse hotspot spanning the heat sink perpendicular to the flow direction resulted in different CHF values based on its streamwise location; CHF was largest when the hotspot was placed nearest the inlet and smallest when placed nearest the outlet. The visualizations revealed that CHF occurs when there is a sudden and unalleviated upstream expansion of vapor in one or more channels above the hotspot, causing the local wall temperature to rapidly increase. The proximity of the hotspot to the inlet manifold, which communicates between all channels and can relieve downstream vapor expansion, appears to determine the resiliency of the heat sink to conditions leading to CHF.

1. INTRODUCTION

The demanding performance, weight, and size constraints placed on modern electronics systems has driven packages and components to take increasingly thinner and more compact form factors; incorporation of relatively thick heat spreaders to mitigate propagation of non-uniformities in heat generation along the thermal resistance pathway is increasingly infeasible as a thermal management strategy in high-performance systems. Instead, non-uniform heat flux profiles must be directly communicated to the heat sink and accommodated therein. Microchannel heat sinks are an excellent choice due to their ability to handle high heat fluxes, but an improved understanding of the effects of non-uniform heating profiles on the heat dissipation limits of microchannel heat sinks is needed to accommodate these thermal packaging trends.

Studies of critical heat flux (CHF) in microchannels were summarized in [1, 2, 3]. These studies have typically investigated critical heat flux using either a single channel [4, 5] or a parallel array of

channels [6, 7]. Although the parameters affecting the critical heat flux under uniform heating conditions are reasonably well understood, realistic applications can impose highly non-uniform heat fluxes [8]. A better understanding of how the location of heated regions (referred to as hotspots in the present work) affects the critical heat flux in two-phase microchannel cooling is needed to reliably predict the performance of heat sinks in actual applications.

Experiments using a single, circular channel were performed by Del Col and Bortolin [5] using three refrigerants. A non-uniform heat flux, first increasing and then decreasing along the flow length, was imposed on the channel. The dryout quality and average critical heat flux were measured during annular flow. The data were compared to several models that were developed for uniformly heated microchannels [2, 9, 10, 11, 12]; the models were found to overpuredict the critical heat flux data.

An experimental investigation by Chen and Garimella [6] considered a parallel array of microchannels. At near-CHF conditions, significant amounts of vapor in some channels were seen to undergo flow reversal into the inlet manifold, thus altering the inlet bulk fluid temperature. Inlet subcooling was shown to have no effect on the critical heat flux, which was instead governed by the vapor backflow. An abrupt decrease in the pressure drop was measured during CHF, and CHF was found to be strongly dependent on the fluid properties and flow rate.

Results from multiple CHF experiments were compared to correlations in the literature to identify the most suitable CHF predictor [11, 13, 14]. Zhang et al. [11] recommended the Hall-Mudawar correlation [15] for subcooled water, while the Shah correlation [16] best predicted CHF for saturated water. Although they developed their own correlation, Zhang et al. [11] recognized its use being limited for uniform heating conditions. Revellin et al. [13] pointed out that the preferred CHF correlation would be based on the fluid used. They concluded that for non-aqueous fluids, the theoretical model by Revellin and Thome [9] best matched extant data, while for water, the correlation by Zhang et al. [11] was most suitable. Other studies have proposed CHF models [9, 12, 17, 18] based on published experimental data. Of these models, none were compared to experimental data for non-uniform heating.

A few recent studies considered the effects of non-uniform heating on flow boiling [19, 20], and showed that local hotspots cause a significant deviation in local wall temperatures, local heat fluxes, and the total power dissipation capability as compared to a uniformly heated case. However, CHF was not investigated in these experimental studies.

In a recent study by the authors, the effects of non-uniform heating profiles in a microchannel heat sink on heat transfer coefficients, wall temperatures, and the location of boiling incipience were investigated [21]. The experimental results showed that the same total power input distributed over different extents of the chip in different locations and configurations significantly changed the local heat fluxes and heat transfer coefficients across the heat sink. Even with a very thin heat sink base, lateral conduction in the base was significant and had to be taken into account when calculating local wall heat fluxes and heat transfer coefficients. In the worst case tested, a central hotspot spanning the length of the heat sink in the streamwise direction and covering 20% of the base area produced a maximum wall temperature that was 14.4% greater than that for a uniform case at the same total power input. Due to limits on the wall temperature that could be allowed on the test chip, CHF was not investigated in [21].

The present work is a follow-up study that focuses on several hotspot configurations to determine their effect on the critical heat flux in a microchannel heat sink. The same heat sink as in [21] was used, but the fluid was changed from FC-77 (boiling point of 97 ºC at 1 atm) to HFE-7100 (boiling point of 61 ºC at 1 atm) so that CHF may be reached at a lower wall temperature without damage to the test piece. Local wall temperatures and heat fluxes are reported and the location of the hotspot is determined to have a significant effect on CHF. This work provides a better understanding of how non-uniform heating profiles change the magnitude and location of critical heat flux as compared to a uniform case.

2. EXPERIMENTAL METHODS

2.1. Test Section

The microchannel test section used in the current study is the same as that described in [21] and is shown as an inset in the flow loop schematic diagram (Figure 1); a summary of the details is provided here for completeness. The working fluid routes through a silicon microchannel heat sink with a base area of 12.7 mm × 12.7 mm via a transparent manifold cover plate made of polycarbonate. The silicon heat sink is mounted directly on a printed circuit board (PCB) that is connected to an electrical quick-connect board; an insulating G10 glass-epoxy composite layer is placed between the PCB and quick-connect board to direct heat into the silicon heat sink. A 0.8 mm-thick silicone rubber sheet is sandwiched between the microchannel heat sink and cover plate to insulate the polycarbonate (rated to a temperature of 115-130 °C) from thermal damage, and forms a seal to prevent cross flow between the channels. The manifold has inlet and outlet header sections, each with a flow length of 10 mm, width of 12.7 mm, and height of approximately 1.4 mm.

The silicon heat sink is manufactured by cutting parallel microchannels into the top surface of a 650 µm-thick chip with a dicing saw. A heat sink with 35 microchannels is used in the current study; the channel width and depth are 240 µm and 370 µm, and the fin width is 110 µm. The channels were cut with multiple passes creating waviness on the bottom channel surface. The average surface roughness of the bottom of the channels is 0.82 µm, while the sides of the channels have a surface roughness of 0.1 µm [22].

A 5 × 5 array of resistance heaters and temperature-sensing diodes is located on the underside of the heat sink. The individual heater resistances of the 25 heaters are comparable, and allow a single voltage to be applied in parallel to produce a uniform flux over the desired area. Connector pins are used to connect a DC voltage power supply to specific heaters to provide customized, non-uniform heating profiles to the underside of the microchannel heat sink. From the applied voltage, the local heat generated by the resistors at each of the 25 diodes is calculated based on a calibration of the resistance of each heater. Local temperatures are calculated based on a calibration of the diode temperature response. Details about the calibration procedures for each sensor are available in [22].

To prevent damage to the test chip while investigating CHF, a cutoff sensor is connected to the power supply. When the sensor detects a chip temperature above a preset threshold, the power supply is almost immediately (within a few milliseconds) disconnected from the heaters. The preset threshold was chosen as the upper limit of safe operating temperatures for the test chip, 140 °C.

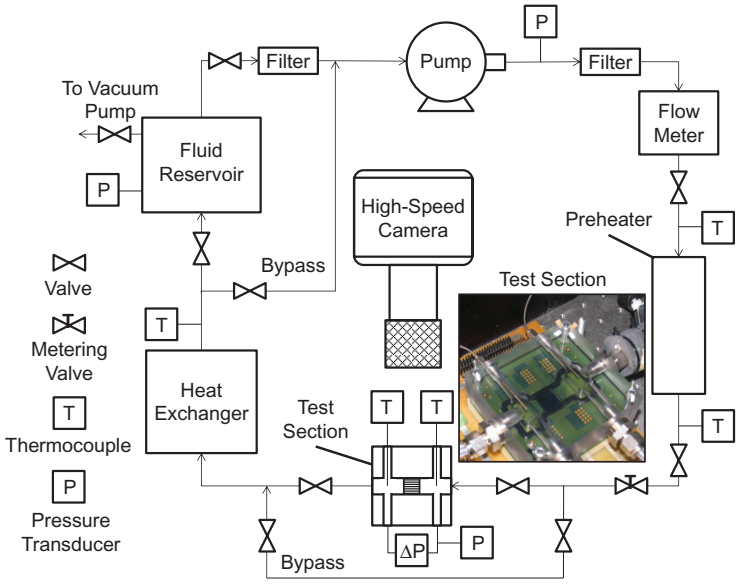

Figure 1. Schematic diagram of the flow loop; a photograph of the microchannel test section is inset.

2.2. Flow Loop

The experimental flow loop is a modified version of that described in [21], and a schematic diagram is shown in Figure 1. A magnetically coupled gear pump (Micropump 415A) circulates the dielectric fluid HFE-7100 through the loop and a preheater warms the fluid to the desired test section inlet temperature. The fluid HFE-7100 was chosen for its low boiling point (61 °C at 1 atm) so that experiments can be run up to CHF within the safe operating temperature range of the test chip; it is noted that this is a different fluid than the FC-77 (boiling point of 97 ºC at 1 atm) used previously for the experiments in [21]. A liquid-to-air heat exchanger is included downstream of the test section to cool the fluid before it reenters the reservoir. The liquid flow rate is measured using a 20-200 mL/min microturbine flow meter (McMillan S-114). The fluid temperature is measured using T-type thermocouples upstream of the preheater, upstream and downstream of the test section, and downstream of the heat exchanger. The inlet pressure is measured using a 0-30 psia pressure transducer (Gems Sensors 2200 series). The pressure drop across the test section is measured using a 0-10 psi differential pressure transducer (Omega PX2300 series).

High-speed videos are captured viewing downwards on the top of the heat sink using a Photron Fastcam Ultima APX high-speed digital video camera combined with a Nikon AF Micro-Nikkor 200 mm IF-ED lens. The microchannel heat sink is illuminated using a Sunoptic Technologies Titan 300 xenon arc lamp. High-speed videos are captured at 8,000 frames per second using a shutter speed of 8 kHz.

2.3. Test Procedure

The fluid is degassed using a vacuum pump connected to an expandable reservoir. The expandable reservoir design is detailed in [23]. At ambient temperature and pressure, HFE-7100 contains 53% air by volume [24]. The expandable reservoir is first fully expanded to create a gas space at the top. The vacuum pump is used to produce a vacuum pressure equal to the vapor pressure of the fluid for 2 min to remove the mixture of air and HFE-7100 vapor that has collected in the gas space. The expanded reservoir is then left at a vacuum pressure for at least one hour to allow the dissolved air to diffuse from the liquid into the gas space. The process is repeated until the vacuum pressure in the reservoir is constant with time, which indicates that air is no longer diffusing out of the liquid. The fluid is then cycled through the flow loop and the process is repeated to ensure that all the air is removed from the system. The fluid is considered fully degassed once the measured fluid temperature at incipience is equal to the saturation temperature of HFE-7100 when boiled in the preheater.

Experiments in the current study are performed at a single mass flux of 797 kg/m^{2}s. Once a constant flow rate is established, the fluid is preheated to a test section inlet temperature of approximately 50.8 °C that remains fixed throughout the test. The expandable reservoir is allowed to expand freely in order to maintain a relatively constant system pressure that is nearly equal to atmospheric pressure.

Power is supplied to individual heating elements to simulate the desired hotspot configurations. The total power supplied to these heating elements is incremented from zero until the critical heat flux is reached. At each power input level, the system is allowed to reach a steady state before the next power level is imposed. When CHF is reached, the local temperature rapidly increases and the cutoff sensor is triggered. When the cutoff is triggered the first time, the total power supplied is noted and the system is reset. After the system is reset, the power input is set to just below the level that first triggered the cutoff, such that CHF can be approached in finer power input increments. After successive repetition of this procedure to arrive at ever finer power increments as CHF is approached, the system is allowed to reach steady state at a heater power level from which any perceptible increase would trigger CHF. This procedure provides an accurate estimation of CHF. Transient measurements upon CHF actually having been reached are not included due to the limited frequency of the chip temperature measurements. High-speed videos of the microchannel heat sink are recorded while CHF is approached to visually capture the phenomenon.

The cutoff sensor conveniently allows repeated activation of critical heat flux using a single test chip without damage. A test chip was sacrificed to demonstrate the damage resulting from the uncontrolled

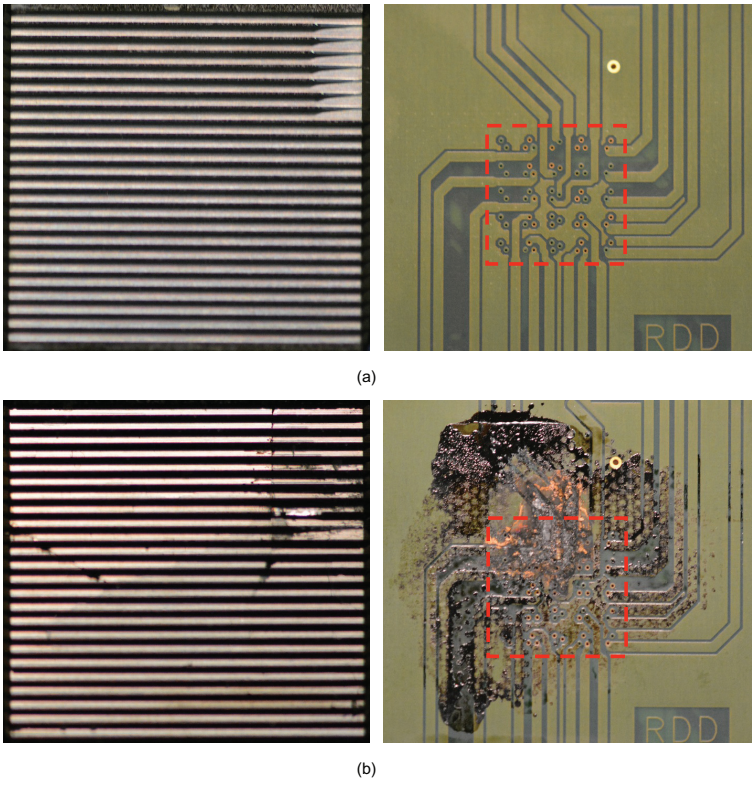

Figure 2. The microchannel heat sink and corresponding backside PCB traces shown for (a) an undamaged test chip, and (b) a test chip damaged after CHF. Red lines indicate the location of the heat sink on the underside of the PCB to scale.

progression of CHF. Fifteen of the temperature sensors were permanently damaged and the silicon heat sink itself was cracked as a result of CHF. Images of an undamaged test piece and a test piece damaged by CHF are shown in Figure 2.

2.4. Data Reduction

Local heat fluxes, wall temperatures, and fluid temperatures are measured at steady state for each test point. The data reduction method is summarized here while a full description is provided in [21]; fluid properties have been updated to account for the change in fluid from FC-77 to HFE-7100. This process takes into account heat spreading that occurs within the heat sink base for cases with non-uniform heating.

The net local heat transfer rate from the microchannel heat sink to the fluid ($\dot{q}_{net}$) is calculated based on an energy balance for each heating element which consists of the energy generated, the heat loss, and lateral conduction between elements as

$$\dot{q}_{net,ij} = \dot{q}_{gen,ij} - \dot{q}_{loss,ij} - \dot{q}_{cond,ij}. \tag{1}$$

The test section heat loss is calibrated as a function of the base temperature. A complete description of the calibration procedure is found in [25]. Lateral conduction that occurs when non-uniform heating profiles are imposed is calculated between elements as

$$\dot{q}_{cond,ij} = k_{Si}\frac{L}{5}(t-d)\frac{\left(4T_{i,j} - T_{i+1,j} - T_{i-1,j} - T_{i,j+1} - T_{i,j-1}\right)}{L/5}, \tag{2}$$

where the total net conduction depends on the four neighboring elements of heater i, j.

The bulk fluid temperature above each heating element in single-phase flow is calculated as

$$T_{f,ij} = T_{in} + \frac{\sum_i \dot{q}_{net,ij}}{GwdN/5c_p}, \tag{3}$$

where $\sum_i \dot{q}_{net,ij}$ represents the sum total of net heat transferred to the fluid from the inlet to the heating element in question. After sensible heating raises the fluid to the saturation temperature, the fluid temperature is then maintained equal to the saturation temperature at the local pressure.

A corrected local wall temperature is calculated based on the measured diode temperature by accounting for conduction through the base of the microchannel heat sink and is calculated as

$$T_{w,ij} = T_{d,ij} - \frac{q''_{b,ij}(t-d)}{k_{Si}}. \tag{4}$$

The local base heat flux is calculated using the local net heat transfer rate as

$$q''_{b,ij} = \frac{\dot{q}_{net,ij}}{A_b/25}. \tag{5}$$

The local heat flux transferred to the fluid is also calculated using the local net heat transfer rate and is based on the wetted area of the channels as

$$q''_{w,ij} = \frac{\dot{q}_{net,ij}}{NL(w+2d)/25}. \tag{6}$$

2.5. Test Cases

A variety of hotspot heating profiles were investigated and are shown in Figure 3. Heaters in the hotspot locations (displayed in red) are turned on while the remainder (displayed in gray) are powered off. The first case is a uniformly heated profile that serves as a basis of comparison for the remaining non-uniform cases. The next three cases correspond to hotspots that span the width of the heat sink in the transverse direction, placed at the inlet, center, and outlet of the flow path. The next case corresponds to a centered hotspot that spans the length of the heat sink in the streamwise direction. The last case corresponds to two transverse hotspots located at the inlet and outlet.

3 RESULTS AND DISCUSSION

The total power input, local heat flux, and maximum wall excess temperature at the critical heat flux are summarized for all cases in Table 1. Selected cases from this table will be analyzed in greater detail in the following paragraphs to illustrate the key effects of non-uniform heating on CHF. In all cases, the local heat flux and wall temperature are greatest above the active heater elements, as expected. The influence of non-uniform heating on the trends in local wall temperatures, heat fluxes, and heat transfer coefficients leading up to CHF was explained in detail in [21]. The current study extends this work by exploring the influence of non-uniform heating on CHF; it is noted that a lower-boiling-point working fluid is used in the current work as discussed earlier.

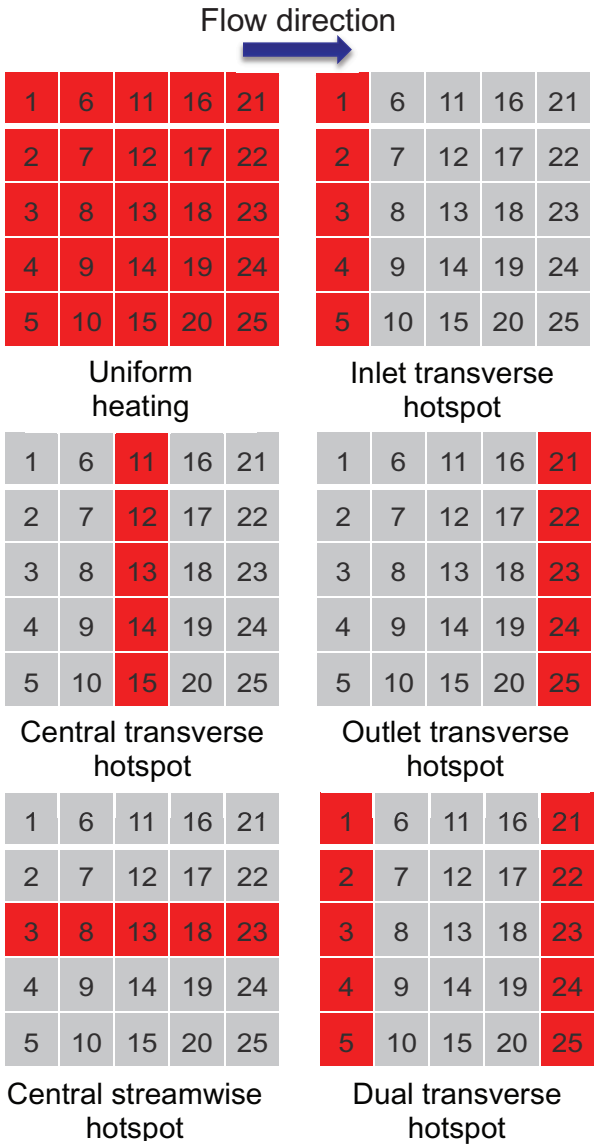

Figure 3. Non-uniform heating profiles investigated in the current study.

Boiling curves for a central transverse hotspot (sensors 11-15) and a central streamwise hotspot (sensors 3, 8, 13, 18, and 23) are shown in Figure 4. These curves are plotted using the local heat flux to the fluid and the local wall excess temperature. For single-phase flow, the wall excess temperature is calculated using the local bulk fluid temperature, while for two-phase flow it is calculated using the saturation temperature at the local pressure.

Table 1. Summary of results for all test cases.

	Total power input at CHF (W)	Local heat flux at CHF (W/cm^2)	Maximum wall excess temperature at CHF (°C)
Uniform	137.2	14.2	67.0
Inlet transverse	57.2	53.4	54.1
Central transverse	61.3	42.8	62.5
Outlet transverse	44.8	29.7	67.4
Central streamwise	34.9	8.7	73.9
Dual transverse	89.7	25.9	65.9

3.1. Central Transverse Hotspot

In the central transverse hotspot case, the wall excess temperature initially increases with a constant slope as the heat flux is increased. This reflects the relatively constant heat transfer coefficient characteristic of single-phase flow. The lines for all heated sensors overlap in this region. Boiling incipience is indicated by a reduction in wall temperature and an increased slope of the lines, and is confirmed by visual observation from the high-speed videos. In the two-phase region, lines corresponding to the three middle sensors overlap (12-14); the two sensors on the boundaries (11 and 15) show a larger wall excess temperature. In this case, CHF occurs above sensor 15 on the boundary; as CHF is approached, a simultaneous decrease in the heat flux to the fluid and increase in wall excess temperature are observed. This behavior aids identification of the general location of CHF for all cases; the exact location is confirmed using visual evidence from the high-speed imaging. Throughout this study, CHF was typically found to occur in a location near the lateral boundaries of the microchannel heat sink (unless that area was not heated). This location can be confirmed for all cases via high-speed images and the changes in the boiling curve (as was demonstrated for the central transverse case here). It is likely that CHF occurs in these locations because of maldistribution caused by the inlet manifold geometry that reduces the flow into these channels [26].

High-speed images during the period where the temperature cutoff is triggered are shown in Figure 5; CHF is determined to occur in the bottommost channel in the images. The images show a portion of the flow length and only the four channels nearest the edge of the heat sink directly above hotspot sensor 15. At time t = 0 ms, the system is at stable operation just prior to the occurrence of CHF. In the bottommost channel in the image, small bubbles nucleate over the hotspot, grow, and are carried downstream. A short time later (t = 44.9 ms), CHF is reached and larger bubbles form in the channel which coalesce to form a long and contiguous vapor region. This vapor region quickly expands in both directions until the channel is almost completely full of vapor (t = 50.5 ms). This sudden vapor expansion causes a local rapid temperature increase and triggers the cutoff sensor built into the experimental setup, shutting off power to the chip. Additionally, the local pressure within the channel increases, preventing liquid from entering the channel, thus resulting in local flow reversal. After the power is cut off and the pressure in the bottom channel has equalized, liquid can again flush the channel and the wall temperature decreases (t = 58.5-82.4 ms). Sudden vapor expansion is characteristic of CHF in all cases; the high-speed videos of the central transverse hotspot case reveal this well and are included as Supplementary Data.

3.2. Central Streamwise Hotspot

Boiling curves for the central streamwise hotspot case are shown in Figure 4b. As in the central transverse hotspot case, a single-phase region with constant slope is observed at low heat inputs. This slope is largest for the heater furthest upstream (sensor 3), corresponding to the higher heat transfer coefficient in the entrance region due to thermally developing flow, and decreases at successive sensor locations downstream. Once again, boiling incipience is indicated when the slope of the lines changes, as is confirmed with observation of the high-speed videos. In the case of this central streamwise

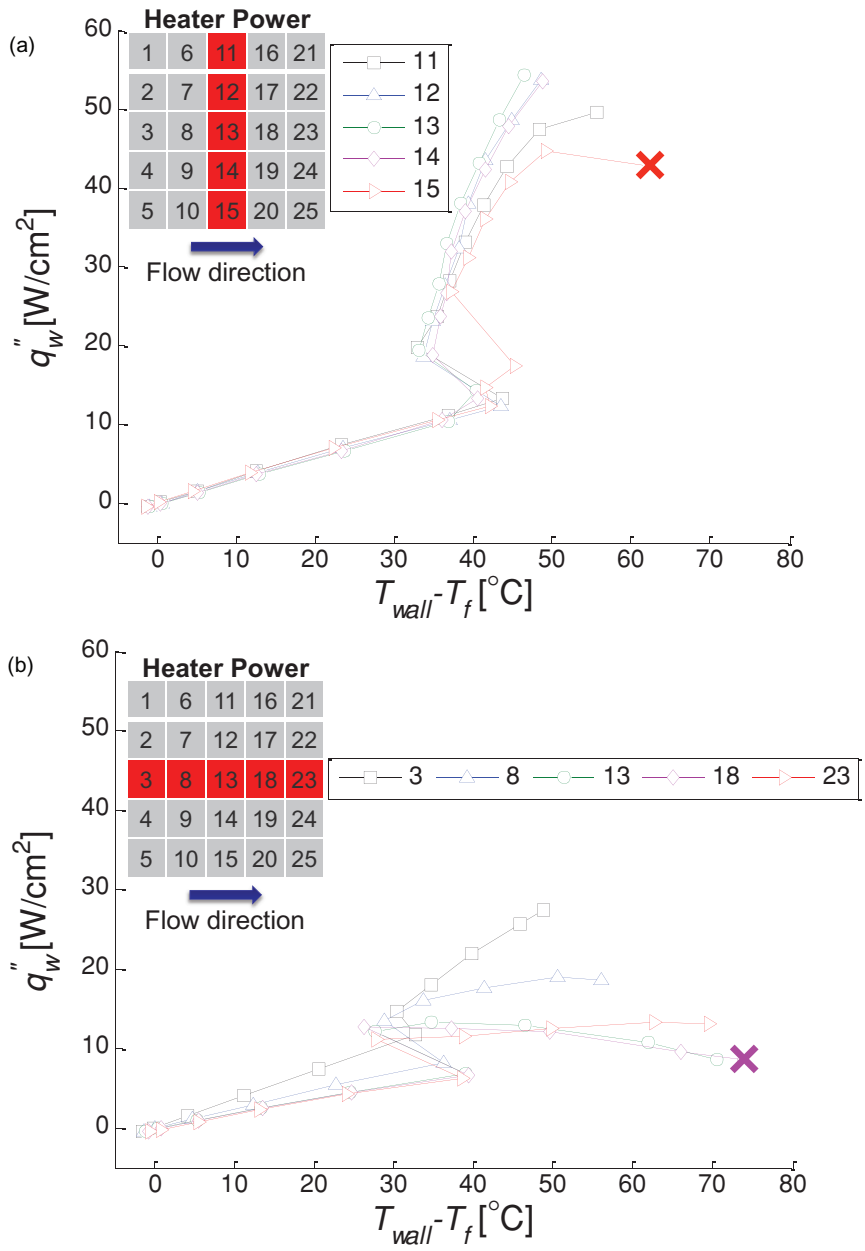

Figure 4. Heat flux transferred to the fluid plotted against the wall excess temperature for (a) a central transverse hotspot, and (b) a central streamwise hotspot. "X" indicates the location of CHF.

hotspot, the temperature rise from sensors 3 to 8 in the upstream portion of the heat sink generally follows the trends for a uniform heating case; in contrast, the location of CHF does not occur at the outlet as would be expected for a uniformly heated case. Rapid vapor expansion leads to a rapid temperature increase (*i.e.*, CHF) slightly upstream of the outlet, above sensor 18. This is reflected in the boiling curve where the largest wall excess temperature is measured at sensor 18 and corresponds with a drop in the heat flux to the fluid. High-speed video evidence for this case also indicates that bidirectional vapor expansion in the channels begins upstream of the outlet, centered over sensors 13

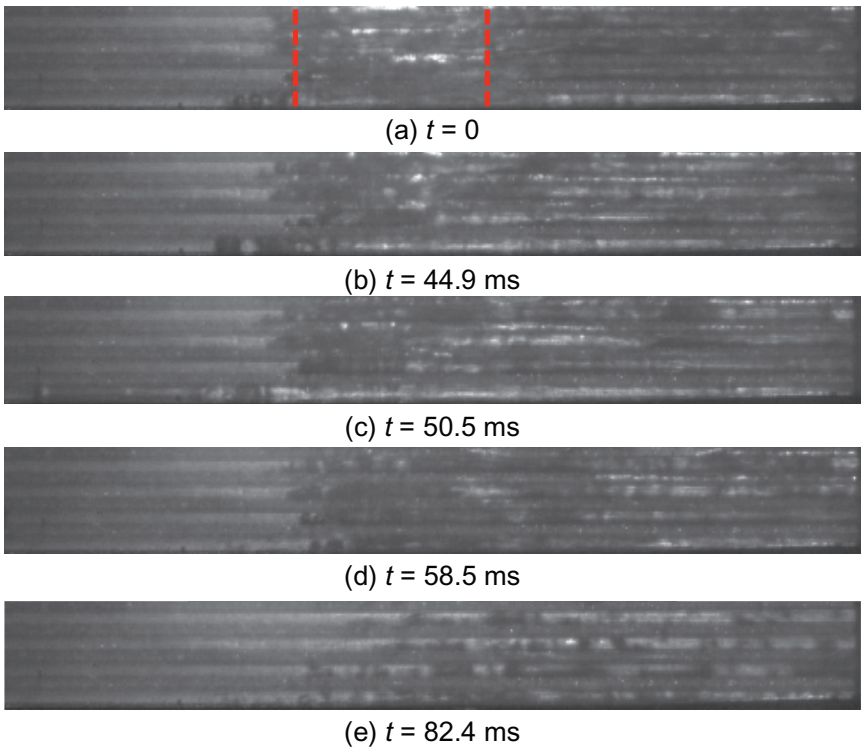

Figure 5. High-speed images recorded at 8000 frames per second for a central transverse hotspot at CHF. Flow goes from left to right; the hotspot is indicated by the red dashed lines. Vapor expands rapidly in the bottommost channel (maximum upstream distance at $t = 50.5$ ms) at CHF before the heater power is cut off.

and 18. In this study, while CHF was always found to occur within the footprint of the hotspot, it does not necessarily occur at the outlet (unlike for a uniform-heating case).

3.3. Effect of Heating Profile on CHF

The boiling curves show that the location where the cutoff sensor is triggered – considered the location where CHF occurs – is strongly dependent on the heating profile. Further interrogation of the data shows that the maximum wall excess temperature at CHF also varies significantly based on the heating configuration, and ranges from 54.1 °C to 73.9 °C, as seen in Table 1. One determinant of these differences is the heat spreading occurring in the substrate. Heat from transverse hotspots is conducted through the silicon substrate in both upstream and downstream directions; streamwise hotspots, on the other hand, spread heat transverse to the flow direction, between channels. Another possible explanation of the differences in CHF location and the associated temperatures is advection of heated fluid to non-heated regions within a channel. Since transverse hotspot cases advect hot fluid into unheated portions of channels, it is expected that a transverse hotspot would see lower maximum wall excess temperatures at CHF as compared to streamwise and uniform heating profiles, where heated fluid continues to flow over downstream heated regions. In general, the wall excess temperatures at CHF for the hotspot cases are lower than that of a uniformly heated case, except for the two cases that contain a heated region at the outlet – a transverse hotspot at the outlet and the dual transverse hotspots – which have wall excess temperatures similar in magnitude to that of a uniformly heated case.

3.4. Effect of Hotspot Location on CHF

To explore the effect of hotspots with the same input heating profile but positioned in different locations of the heat sink, a transverse hotspot was investigated at inlet, central, and outlet locations along the microchannel flow path. The differences between these three cases are summarized in Table 1. The highest total power that can be dissipated (61.3 W) at critical heat flux occurs when the hotspot is located in the center (not to be confused with the highest local *wall* heat flux at CHF). This is because the ability for heat spreading in both directions (upstream and downstream) to unheated regions of the heat sink allows for greater total heat dissipation from the central transverse hotspot relative to the inlet and outlet hotspots, whose locations limit heat spreading to one direction. When the hotspot is moved to the outlet or inlet, CHF is reached at a lower total power input.

The local wall heat flux based on the wetted wall area at CHF itself also varies based on the streamwise location of the transverse hotspot, and is indicative of the different hydrodynamics for each location at CHF. Temperature and wall heat flux maps of the three transverse hotspot cases at CHF are shown in Figure 6. The location where CHF occurs is marked with an "X". When the hotspot is located at the outlet, the local critical heat flux is the lowest of the three cases at 29.7 W/cm^2. When the hotspot is at the inlet, the local critical heat flux of 53.4 W/cm^2 is the highest for all the cases tested. In general, the critical heat flux decreases as the hotspot moves downstream, and the wall excess temperature increases. The reason for this behavior is related to the ability of the fluid at the location of the hotspot to communicate with the inlet manifold. When the hotspot is located at the inlet, quickly expanding vapor regions are more easily able to reverse into the manifold, which allows fresh liquid to enter the channel before the rapid temperature rise can induce CHF. When the hotspot is located further downstream, travel upstream to the inlet manifold of rapidly expanding vapor is less easily accommodated. In the current study, the expanding vapor region was never observed to reach the inlet manifold from either the central or outlet transverse hotspots; the critical heat fluxes are hence decreased compared to the inlet case.

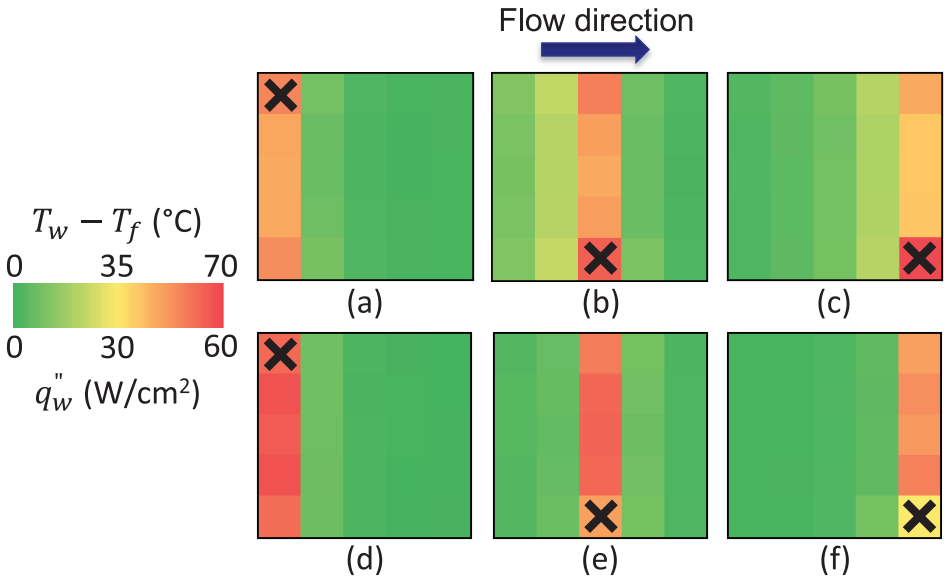

Figure 6. Wall excess temperature map for (a) inlet transverse, (b) central transverse, and (c) outlet transverse hotspot heating cases at CHF. Heat flux map for (d) inlet transverse, (e) central transverse, and (f) outlet transverse hotspot heating cases at CHF.

4. CONCLUSIONS

The effects of non-uniform heat input profiles on the critical heat flux (CHF) in a microchannel heat sink were investigated; details of the non-uniformity in heating influence where the CHF occurs as well as the magnitude of heat flux and local temperature under CHF conditions. Local wall temperatures, local wall heat fluxes, and total power input were measured using an array of embedded temperature sensors. High-speed imaging allowed for visual observation of the CHF phenomenon. Hotspots that spanned the width or length of a silicon microchannel heat sink were investigated by increasing the supplied input power until CHF was achieved.

In terms of the total power input necessary to reach CHF, a central streamwise hotspot was the worst case tested. Transverse hotspots generally allowed for a larger total power dissipation than a streamwise hotspot at CHF; the maximum power input is dissipated at CHF when a transverse hotspot is located halfway along the flow length, due to the capability for heat spreading both in upstream and downstream directions. It was found that the central streamwise case yielded the lowest critical heat flux and largest maximum wall excess temperatures at CHF in comparison to all the transverse cases. A streamwise hotspot extending over the entire flow length creates flow maldistribution among the channels. The transverse hotspot cases produced higher critical heat fluxes and lower maximum wall excess temperatures at CHF; the critical heat flux decreased and temperature increased as the hotspot moved from the inlet to the outlet. The high critical heat flux and low wall excess temperature that occurs when the hotspot is located at the inlet is attributed to the ability for expanding vapor regions to communicate with the inlet manifold.

The critical heat flux was identified from its signature on the boiling curves, and gave rise to a rapidly increasing local wall temperature that tripped a power supply cutoff sensor; the location of critical heat flux was confirmed via high-speed movies. A rapid vapor expansion in one or more channels at the hotspot location led to CHF. The location of CHF depended on the heating configuration, and CHF only occurred within the footprint of the hotspot. Furthermore, in the current study, CHF typically occurred in channels within the regions of the hotspot located on the lateral boundaries of the heat sink. The repeatable occurrence of CHF in these same channel locations is likely due to slight flow maldistribution caused by the inlet manifold geometry. Thus, the location of CHF can be anticipated based on a combination of the heating profile and flow maldistribution between the channels.

ACKNOWLEDGEMENTS

Financial support for this work was provided by the Cooling Technologies Research Center, a National Science Foundation Industry/University Cooperative Research Center at Purdue University. The authors thank Bruce Myers of Delphi Electronics and Safety, Kokomo, Indiana for providing the silicon microchannel heat sink test chip.

SUPPLEMENTARY DATA

A supplementary video is provided for Figure 5 that shows the vapor flow behavior at CHF for a central transverse hotspot.

NOMENCLATURE

	heat sink base area (m^2)
	specific heat ($J\ m^{-2}K^{-1}$)
	microchannel depth (m)
	mass flux ($kg\ m^{-2}s^{-1}$)
	thermal conductivity of silicon ($W\ m^{-1}K^{-1}$)
	heat sink width (m)
	number of microchannels, heaters
	base heat flux ($W\ m^{-2}$)
	heat conduction (W)

heat generation (W)
heat loss (W)
total heat transferred to the fluid (W)
wall heat flux (W m^{-2})
diode temperature (C)
fluid temperature (C)
inlet fluid temperature (C)
wall temperature (C)
heat sink thickness (m)
microchannel width (m)

Subscripts

heater element in the flow direction
heater element in the transverse direction

REFERENCES

[1] Roday, A.P. and Jensen, M.K., A review of the critical heat flux condition in mini- and microchannels, *Journal of Mechanical Science and Technology*, 2009, 23, 2529-2547.

[2] Kandlikar, S.G., History, advances, and challenges in liquid flow and flow boiling heat transfer in microchannels: A critical review, *Journal of Heat Transfer*, 2012, 134, 034001.

[3] Tibirica, C.B., and Ribatski, G., Flow boiling in micro-scale channels – synthesized literature review, *International Journal of Refrigeration*, 2013, 36, 301-324.

[4] Wojtan, L., Revellin, R. and Thome, J.R., Investigation of saturated critical heat flux in a single, uniformly heated microchannel, *Experimental Thermal and Fluid Science*, 2006, 30, 765-774.

[5] Del Col, D. and Bortolin, S., Investigation of dryout during flow boiling in a single microchannel under non-uniform axial heat flux, *International Journal of Thermal Sciences*, 2012, 57, 25-36.

[6] Chen, T. and Garimella, S.V., A study of critical heat flux during flow boiling in microchannel heat sinks, *Journal of Heat Transfer*, 2012, 134, 011504.

[7] Kosar, A., Peles, Y., Bergles, A.E., and Cole, G.S., Experimental investigation of critical heat flux in microchannels for flow-field probes, in: *ASME Seventh International Conference on Nanochannels, Microchannels, and Minichannels*, Pohang, South Korea, June 22-24, 2009, Paper No. ICNMM2009-82214.

[8] Hamann, H.F., Weger, A., Lacey, J.A., Hu, Z., Bose, P., Cohen, E. and Wakil, J., Hotspot-limited microprocessors: direct temperature and power distribution measurements, *IEEE Journal of Solid-State Circuits*, 2007, 42, 56-65.

[9] Revellin, R. and Thome, J.R., A theoretical model for the prediction of the critical heat flux in heated microchannels, *International Journal of Heat and Mass Transfer*, 2008, 51, 1216-1225.

[10] Katto, Y., and Ohno, H., An improved version of the generalized correlation of critical heat flux for the forced convective boiling in uniformly heated vertical tubes, *International Journal of Heat and Mass Transfer*, 1984, 27, 1641-1648.

[11] Zhang, W., Hibiki, T., Mishima, K. and Mi, Y., Correlation of critical heat flux for flow boiling of water in mini-channels, *International Journal of Heat and Mass Transfer*, 2006, 49, 1058-1072.

[12] Kosar, A., A model to predict saturated critical heat flux in minichannels and microchannels, *International Journal of Thermal Sciences*, 2009, 48, 261-270.

[13] Revellin, R., Mishima, K. and Thome, J.R., Status of prediction methods for critical heat fluxes in mini and microchannels, *International Journal of Heat and Fluid Flow*, 2009, 30, 983-992.

[14] Tibirica, C.B., Felcar, H.O.M., and Ribatski, G., An analysis of experimental data and prediction methods for critical heat fluxes in micro-scale channels, in: *5th European Thermal-Science Conference*, Eindhoven, Netherlands, May 18-22, 2008.

[15] Hall, D.D. and Mudawar, I., Critical heat flux (CHF) for water flow in tubes – II. Subcooled CHF correlations, *International Journal of Heat and Mass Transfer*, 2000, 43, 2605-2640.

[16] Shah, M.M, Improved general correlation for critical heat flux during upflow in uniformly heated vertical tubes, *International Journal of Heat and Fluid Flow*, 1987, 8, 326-335.

[17] Revellin, R. and Thome, J.R., Critical heat flux during flow boiling in microchannels: a parametric study, *Heat Transfer Engineering*, 2009, 30, 556-563.

[18] Kandlikar, S.G., A scale analysis based theoretical force balance model for critical heat flux (CHF) during saturated flow boiling in microchannels and minichannels, *Journal of Heat Transfer*, 2010, 132, 081501.

[19] Costa-Patry, E. and Thome, J.R., On-chip cooling of hot-spots with a copper micro-evaporator, in: *28th Annual IEEE Semiconductor Thermal Measurement and Management Symposium (SEMI-THERM)*, San Jose, CA, March 18-22, 2012.

[20] Liu, C.K., Yang, S.J., Chao, Y.L, Liou, K.Y. and Wang, C.C., Effect of non-uniform heating on the performance of the microchannel heat sinks, *International Communications in Heat and Mass Transfer*, 2013, 43, 57-62.

[21] Ritchey, S.N., Weibel, J.A. and Garimella, S.V., Local measurement of flow boiling heat transfer in an array of non-uniformly heated microchannels, *International Journal of Heat and Mass Transfer*, 2014, 71, 206-216.

[22] Harirchian, T. and Garimella, S.V., Microchannel size effects on local flow boiling heat transfer to a dielectric fluid, *International Journal of Heat and Mass Transfer*, 2008, 51, 3724-3735.

[23] Chen, T. and Garimella, S.V., Effect of dissolved air on subcooled flow boiling of a dielectric coolant in a microchannel heat sink, *Journal of Electronic Packaging*, 2006, 128, 398-404.

[24] 3M, 2002, "3M Novec Engineered Fluid HFE-7100 for Heat Transfer", 3M, St. Paul, MN, pp. 1-8.

[25] Chen, T. and Garimella, S.V., Measurements and high-speed visualization of flow boiling of a dielectric fluid in a silicon microchannel heat sink, *International Journal of Multiphase Flow*, 2006, 32, 957-971.

[26] Jones, B.J., Lee, P.S. and Garimella, S.V., Infrared micro-particle image velocimetry measurements and predictions of flow distribution in a microchannel heat sink, *International Journal of Heat and Mass Transfer*, 2008, 51, 1877-1887.